Research Article DOI: https://doi.org/10.64862/ajeg.2025.202.03.269 Open Access

Study on Spatio-Temporal Changes in River Dynamics and Land Cover along the Seti River Floodplain, Kaski, Nepal

Bikash Adhikari[1], Aastha Singh Bhandari[2], Ram Chandra Tiwari[3*] and Aanchal Tiwari[4]

[1,2]Department of Environmental Science and Engineering, Kathmandu University, Nepal
[3,4]Department of Civil Engineering, Institute of Engineering, Pulchowk Campus, Tribhuvan University, Lalitpur, Nepal

(*Corresponding E-mail: rct2075ce_rctiwari@pcampus.edu.np)

Received: August 14, 2025, Accepted: December 22, 2025

Abstract: **In a geographically diverse country like Nepal, changes in river dynamics and land use/land cover are common phenomena. Kaski District, located in the hilly region of central Nepal, exhibits significant variations in river morphology and landform characteristics over time. This study analyzes the decadal changes in river dynamics and land cover along the Seti floodplain from 1989 to 2017 using Geographic Information System (GIS) and Remote Sensing (RS) techniques. Landsat images from four decades were used, followed by radiometric correction, reclassification, and combination for analysis. River dynamics were evaluated through parameters such as sinuosity and bankline shift, while land cover classification employed unsupervised segmentation and indices-based methods. Six land cover categories were identified: water body, built-up area, barren land, agriculture and grassland, shrub and forest, and snow and glacier. The Seti River showed a decreasing trend in sinuosity, with the highest value in 1989 and the lowest in 2017. The maximum bank shift of 42.7 m occurred in the mid-right bank between 1999 and 2009, while the minimum shift of 6.7 m was observed in the upper right bank between 1989 and 1999. Water body area increased from 7.60 km^2 in 1989 to 8.34 km^2 in 2017, and built-up area expanded from 32.44 km^2 to 80.98 km^2. Barren land decreased from 353.80 km^2 to 332.07 km^2, while agriculture and grassland increased from 251.21 km^2 to 320.15 km^2. Shrub and forest areas declined from 984.75 km^2 to 889.05 km^2, whereas snow and glacier cover increased from 458.05 km^2 to 477.55 km^2.**

Keywords: ***Land Use and Land Cover change (LULC), Seti floodplain, Remote sensing and GIS, Bankline shift, Spatio-temporal changes***

Introduction

Nepal River dynamics refers to the study of water and sediment movement within a river channel and its adjacent areas, focusing on how natural processes and human activities influence channel morphology (Hazarika et al., 2015). Natural phenomena such as earthquakes and floods, along with anthropogenic interventions, often modify river behavior, affecting sediment transport, erosion, and deposition patterns. Understanding river dynamics is crucial for predicting channel deformation, assessing associated hazards, and managing floodplains effectively.

Floodplains, defined as low-lying lands adjacent to rivers that experience periodic flooding, serve vital ecological and socio-economic functions. They provide fertile soil for agriculture, habitats for biodiversity, and space for human settlement, especially in densely populated regions of South and Southeast Asia (Hazarika et al., 2015). However, floodplains are dynamic systems constantly reshaped by lateral and vertical river movements, which in turn influence land use and land cover (LULC) patterns.

In the current study, the Seti River in Kaski District, Nepal is taken into account to identify decadal changes in the dynamics of the river and land use/land cover (LULC) from 1989 to 2017. The Seti River passes through major settlement areas such as Pokhara, serving livelihoods, agricultural activities, and water needs. Even after being so important, little effort has been made to assess its geomorphological, ecological, and LULC change aspects. Thus, the main objectives of the study are: (1) to identify the decadal changes in sinuosity and bank shift of the Seti River using GIS and remote sensing technology; (2) to map and analyse the decadal LULC changes of Kaski District from 1989 to 2017; and (3) to highlight the spatial and temporal changes and their relationship with natural and anthropogenic drivers. The current study aims to contribute to the scientific knowledge of river morphology evolution and landscape transformation of the basin. The results of the research can be used for flood hazard prediction and land management, as well as policy-making. The limitations of the study include low resolution of satellite data and lack of field data for validation. The findings provide baseline spatial information for future studies in the Seti River basin.

River dynamics and land use land cover (LULC) pattern

River dynamics phenomena

The study of river flow, sediment transport, and channel evolution has been ongoing for centuries. However, the scientific foundation of river dynamics was established when DuBoys (1879) introduced a bed-load formula and

Rouse (1937) described suspended sediment distribution, advancing river dynamics as a distinct discipline (Wu, 2007). Since then, numerous studies have enhanced understanding in river engineering and floodplain management.

Human activities such as dam construction, channel modification, and land-use change have significantly altered river systems. Müller (1996) observed that engineering interventions disrupted natural morphodynamics and floodplain vegetation, leading to habitat loss and reduced biodiversity. Restoration and conservation efforts therefore emphasize re-establishing natural river processes. Similarly, Dufour et al. (2015) found that anthropogenic control along the Magra River after WWII caused channel narrowing and morphological changes, shifting from braided to meandering patterns and affecting riparian landscapes.

Urbanization increases impervious surfaces, reducing infiltration and enhancing surface runoff. Petchprayoon et al. (2010) noted that urban land expansion along the Yom River accelerated peak-flow discharge, elevating flood risks compared to rural basins.

Shrestha (2010) reported that decreased precipitation in the Bagmati River basin reduced stream power and discharge, increasing sinuosity. Global warming is expected to further alter rainfall patterns, causing intensified floods or river drying (Hassan et al., 2016).

Vegetation strongly influences runoff and erosion. Matheussen et al. (2000) found that reduced forest cover and lower leaf area index increased snow accumulation and runoff in the Columbia River Basin. Similarly, Kalliola and Puhakka (1988) observed that riparian vegetation along Finland's Kamajohka River was shaped by fluvial processes, with primary successions continually renewed by erosion and deposition.

Land use and land cover (LULC) pattern

Land cover change is a global phenomenon driven by both natural and anthropogenic activities, resulting in temporal and spatial modifications of land features (Zewdu et al., 2016). These changes influence surface characteristics such as albedo, roughness, leaf area index, soil texture, and structure (Lambin et al., 2003). Analyzing LULC provides baseline data to understand past land-use patterns, climate change impacts, and human-induced environmental changes.

Urbanization is a major force altering LULC patterns (Xiao et al., 2006). Deng et al. (2009) reported that in Hangzhou, China, 27.4% of land transformed within a decade, primarily from agricultural to urban use. Similarly, Mohan et al. (2011) found that Delhi's population growth and unplanned expansion led to a 16.86% increase in built-up area at the expense of agricultural and open lands. Land-use changes also influence river systems. Klocking and Haberlandt (2002) found that afforestation and valley-floor restoration affected water availability in the Elbe Basin. In the Brahmaputra floodplain, Hazarika et al. (2015) observed that unstable river courses caused significant erosion and deposition, altering settlement and agricultural areas. Such changes highlight the interplay between river dynamics and human adaptation in flood-prone regions.

Walker and Homma (1996) showed that in the Brazilian Amazon, land concentration, rural violence, and deforestation were closely linked. Land-use dynamics are thus not only environmental but also deeply social, demanding consideration of ecological sustainability to ensure social well-being.

Tools for river dynamics and indices used for LULC

Tools for river dynamics

Remote sensing is a technique for obtaining information about the Earth's surface without direct contact. It involves sensing and recording reflected or emitted energy, followed by processing, analysis, and interpretation of the data (Barnsley, 1999). Remote sensing is widely used for mapping, monitoring, and managing natural hazards as well as studying land cover and river dynamics. Commonly used remote sensing software includes ERDAS IMAGINE, eCognition Developer, OSSIM, InterImage, E-foto, and ILWIS.

A Geographic Information System (GIS) is a computer-based technology used for capturing, storing, manipulating, analyzing, and displaying spatial or geo-referenced data (Burrough and McDonnell, 1998). In the study of land and river dynamics, GIS enables the creation of interactive map overlays that support developmental planning, resource management, and hazard assessment. Widely used GIS software includes ArcMap, ArcView, Arc/Info, GRASS GIS, QGIS, and MapInfo.

Indices used for LULC

Various indices are used for the proper delineation of land cover in GIS. NDVI is a simple graphical indicator used to determine whether the target being observed contains live green vegetation or not. Generally, plants show low reflectance in the blue and the red portion of the spectrum because of chlorophyll absorption (Wang et al., 2005). However, they have a slightly high reflectance in green, hence, appearing green to our eyes. Spectral reflectance of a crop varies substantially in the near infrared region (λ=700-1300nm) and in the visible red range (λ=550-700nm) of the electromagnetic spectrum. The plant surface strongly reflects near infrared radiant energy and the properties of the leaf tissues like cellular structure, and the air-cell wall-protoplasm-chloroplast interfaces are the key determinant of the reflectance amount. The NDVI is hence calculated from reflectance measurements in

the red and near infrared (NIR) region of the spectrum by the following relation.

$$NDVI = \frac{R_{NIR}-R_{Red}}{R_{NIR}+R_{Red}} = \frac{Band_4-Band_3}{Band_4+Band_3} \quad (1)$$

Where R_{NIR} is the reflectance of NIR radiation and RRED is the reflectance of visible red radiation (Govaerts and Verhulst, 2010).

The main purpose of NDSI is to identify the snow cover from a given target imagery. Snow has high reflectance in the visible and near-infrared region of the spectrum. However, it can decrease with age of the snow and contamination by aerosols, soot, pollen, etc., yet its reflectance is higher than any other surfaces. It has a high absorbance in infra-red part, resulting in low reflectance. Based on these reflectance properties the MODIS snow cover algorithm was made. The NDSI is hence calculated from reflectance measured in the green and shortwave infrared (SWIR) region of the spectrum by the following relation.

$$NDSI = \frac{R_{Green}-R_{SWIR}}{R_{Green}+R_{SWIR}} = \frac{Band_2-Band_5}{Band_2+Band_5} \quad (2)$$

Where R_{Green} is the reflectance of visible green radiation and R_{SWIR} is the reflectance of shortwave infrared radiation (Riggs et al., 1994).

The Normalized Difference Water Index (NDWI) serves as an indicator to delineate open water features and enhance their presence in remotely sensed images. The reflectance of near infrared radiation and visible green light are operated to delineate the water features while eliminating the presence of soil and terrestrial vegetation features side by side. It may also provide the turbidity estimations of the water bodies (McFeeters, 1996). The NDWI is hence calculated from reflectance measured in the green and near infrared (NIR) region of the spectrum by the following relation.

$$NDWI = \frac{R_{Green}-R_{NIR}}{R_{Green}+R_{NIR}} = \frac{Band_2-Band_4}{Band_2+Band_4} \quad (3)$$

Where R_{Green} is the reflectance of visible green radiation and R_{NIR} is the reflectance of near infrared radiation. The observed river changes, vegetation loss, and urban expansion increase flood and erosion risks, highlighting the need for regular monitoring and sustainable management.

Material and method

Study area

Kaski district is located in the Gandaki region of the Western Development Region of Nepal (Figure 1) and falls under Province 4. It lies between 28.2622° N latitude and 84.0167° E longitude, covering an area of 2,017 km^2. The district's elevation ranges from 450 m to 8,901 m above sea level. The administrative center and district headquarters is Pokhara.

Kaski district majorly has upper tropical climate. Its annual rainfall is around 3876mm. However, the pattern was fluctuating between 1985 and 2013 A.D. The minimum average annual temperature ranges from 0.5 to 5.5˚C while the yearly maximum average temperature has fluctuated from 33 to 37.4˚C (AEPC, 2017).

Vegetation in Kaskivary according to its altitude. Sub-tropical zone (1000-1800masl) is rich in Schimawallichii and Castanopsisindica vegetation type. Other trees like oak, birch, maple, alder are also found. Riverine forests are mostly dominated by simal (Bombaxmalbaricum). On slopes above 1800m evergreen coniferous forests are found containing pine, fir, spruce and larch trees. Rhododendron species occupies the main temperate zone forest at an altitude between 1800-4000masl. The alpine region includes plant species like Juniperusrecurva, Ephedra gerardiana, Rhododendron lepidotumetc (HIMALDOC, 2017).

Kaski is rich in multiple cultures,language and religion. According to the census of 2068 B.S. Kaski has 84 castes, 44 languages and 11 religions. The major ethnic group includes Gurung, Brahmin, Chhetri, Newar, Thakali and Kumal. The major sources of income include agriculture, business and tourism.

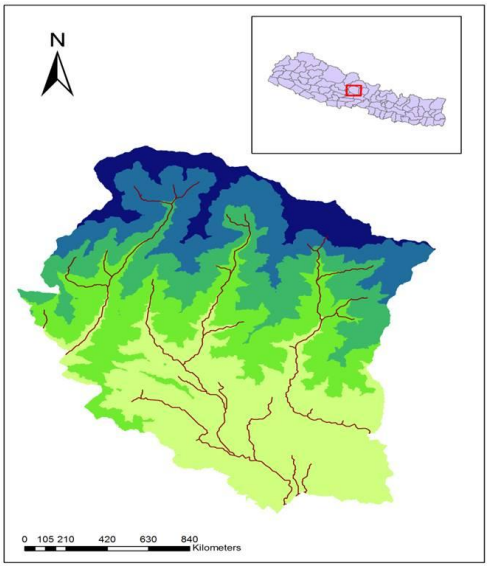

Figure1, Study area- Kaski district with its drainage patterns

Data Collection

Images with least cloud cover were extracted from the official site of U.S Geological Survey. Satellite images of years 1989, 1999, 2009 and 2017 were downloaded. Further information was obtained from related corresponding articles, reports, publications, books, literatures from various sources like a University library, ICIMOD library, HICCDRC, Department of Hydrology and Meteorology and World Wide Web. After the collection of all the desired data and information, they were analyzed using tools like Remote Sensing and GIS.

Landsat images for the stated years, i.e. 1989, 1999, 2008, 2017 were downloaded from the official site of the U.S. geological survey. Best images from the dry season

were selected to obtain images with least cloud cover and also to avoid the overestimation of the river channel. Landsat sensors L4-5 and L8 OLI/TIRS were used. Information about the Landsat images used for the study is given below in Table 1.

Table 1, Detail Information of the Landsat used

Year	Sensor	Acquisition date	Path/Row	Res. (m)
1989	L4-5 TM	7th Nov	142/40	30<10%
1999	L4-5 TM	13th Dec	142/40	30<10%
2009	L4-5 TM	15th Feb	142/40	30<10%
2017	L8 OLI/TIRS	21st Feb	142/40	30<10%

Image processing

The acquired raw images were unzipped and hence processed in QGIS at initial. Pre-processing basically refers to radiometric corrections which involves correction of digital numbers (DN) of the images. It is carried out in order to improve the interpretability and quality of remotely sensed data (Radiometric Corrections).

The sensors, Landsat Thematic Mapper ™ and Enhanced Thematic Mapper (ETM+) after capturing the reflected solar energy, convert the data to radiance. Later they are rescaled into 8-bit digital numbers (DN). These DN can be converted to Top of Atmosphere (ToA) radiance first and ToA reflectance later. Hence, the radiance correction at ToA was carried out using the algorithm.

$$ToA(\lambda) = M_L * Q_{cal} + A_L \qquad (4)$$

Where M_L=Band specific multiplicative rescaling factor from Landsat Metadata, A_L= Band-specific additive rescaling factor from Landsat Metadata and Q_{cal}=Quantized and calibrated standard product pixel values (DN).

After the computation of ToA radiance, reflectance correction at ToA was operated. The following algorithm was used.

$$ToA(\rho_p) = (\pi * L_\lambda * d^2)/(ESUN_\lambda * cos\theta_s) \qquad (5)$$

Where L_λ= Spectral radiance at the sensor's aperture (at-satellite radiance), d=Earth-sun distance in astronomical units, $ESUN_\lambda$= mean solar exo-atmospheric irradiances and θ_s= Solar zenith angle in degrees. The Landsat OLI sensor, however, converts the DN data directly to reflectance compared to TM and ETM+ where two steps computation of radiance and reflectance needs to be carried out.

In order to derive wind, vapor, cloud, rain, and SST products the brightness temperatures are used at remote sensing. This is one of the important radiometric corrections to improve the quality of the image. The conversion of DN to At-Satellite Brightness Temperature is given by the following relation.

$$T_B = k_2/ln[(\frac{k_1}{L_\lambda}) + 1] \qquad (6)$$

Where k_1=Band-specific thermal conversion constant (in watts /meter squared*ster*μm) and k_2= Band-specific thermal conversion constant (in kelvin) and L_λ is the Spectral Radiance at the sensor's aperture measured in watts (meter squared*ster*μm).

After the completion of radiometric corrections, False Color Composite (FCC) was employed for better visualization.

The characteristics of local features such as color, texture, edge and contour are naturally ambiguous. They do not really show the same level of homogeneity or notability at the same spatial scale (Yang et al., 2008). After the preprocessing of the images, Kaski district was clipped from the entire Landsat image with the help of projected shape file of the district. Then an unsupervised segmentation method was operated in ArcMap 10.3 in which the colors of the image were quantized to several representative classes that could be used to differentiate various regions in the image. With the help of image pixels, corresponding color class labels were formed hence forming the class map of the image.

Three main indices were further employed for proper delineation of the land features in Table 2.

Table 2, Main indices employed for the proper delineation of the land features

Index used	Equation
Normalized Difference Vegetation Index	$DVI = \frac{Band4 - Band3}{Band4 + Band3}$
Normalized Difference Snow Index	$NDSI = \frac{Band2 - Band5}{Band2 + Band5}$
Normalized Difference Water Index	$NDWI = \frac{Band2 - Band4}{Band2 + Band4}$

Finally, individually operated raster dataset was combined into a single raster dataset. After the classification, 3x3 Majority Filter was run for further editing using ArcMap tools. This tool basically replaces cells in a raster based on the majority of their adjoining neighboring cells.

Finally, the raster was converted to polygon and some manual editing was carried out as a final touch prior to image analysis.

The area of each individual polygon representing a single class was summed using ArcMap tools. Hence area for each class was obtained. The detail working procedure is included in the flow chart (Figure 2).

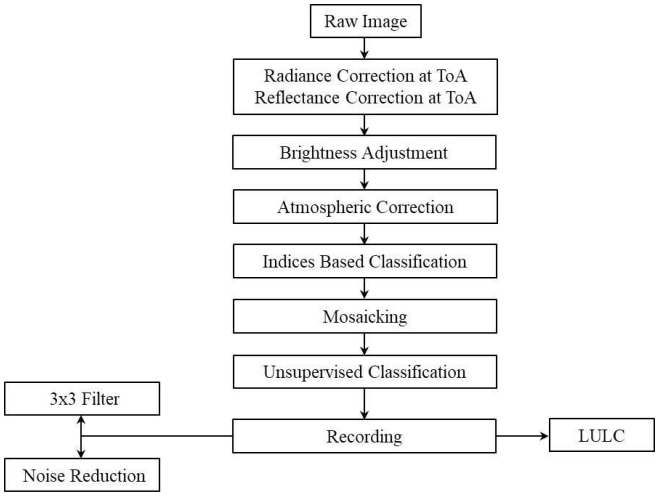

Figure 2, Flow chart of the methodology

Change in River dynamics

Iso-cluster unsupervised classification was used to perform the classification process in the raster band, hence classifying the image and enabling us to locate the desired feature, i.e. River .

With the help of reclassify tool, the classified image was further processed in order to distinguish river course and extract it eventually (Figure 3). With the help of conversion tools, the obtained river raster was ultimately converted to polygon. Manual editing was done to enhance the river features. Ultimately, the river polygon was converted into polylines, and hence bank lines were delineated.

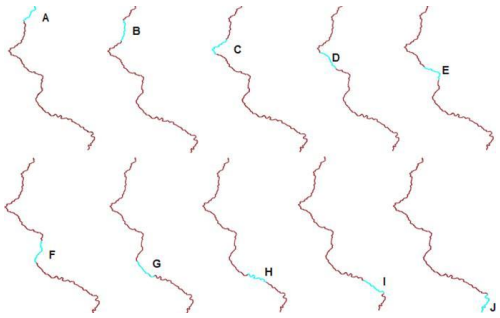

Figure 3, Sections of River

With the help of the obtained bank lines, the channel centerline was generated through detailed on-screen digitization using GIS tools. To ensure a more systematic and unbiased assessment of river dynamics, the entire river channel was divided into ten nearly equal segments for analysis (Hazarika et al., 2015). The sinuosity index and bank line shift were then measured for each segment, allowing a comparative evaluation of channel migration, curvature variation, and the degree of lateral shifting along different reaches of the river.

The extent to which a river channel departs from a straight line is known as river sinuosity (Ebisemiju, 1994). It is calculated as follows.

$$Sinuosity\ (S) = \frac{L}{l} \qquad (7)$$

Where L=Total length of a reach and l= length of straight line between the two points. For the analysis of bank shift, first, points were created on the vertices of the bank. Then, minimum distance between the vertices and next bank (corresponding to the bank with vertices) was calculated. Suppose, points were created on the vertices of the left bank of 1989, then the nearest distance between those vertices and left bank of 1999 bank was calculated. Then again points were created on 1999 bank and minimum distance was measured with 2009 bank and so on. The same process was continued for the right bank. Hence, the entire shift in each segment of each bank was obtained, along with sinuosity.

Result and discussion

After the application of the radiometric corrections, clear and good quality images were obtained for the analysis (Figure 4).

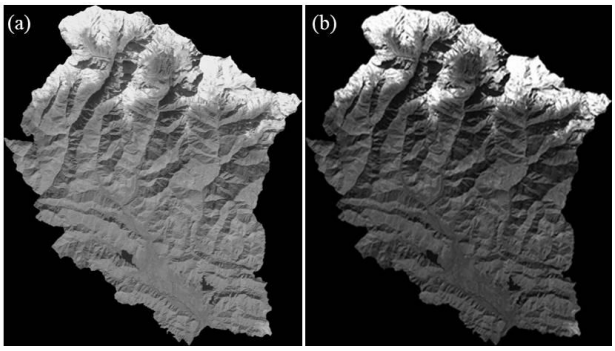

Figure 4, Image correction: (a) Before and (b) After.

Sinuosity of Seti

Since the river was divided into 10 sections, sinuosity for both banks in each section was obtained. Section A refers to the uppermost part of the river channel where the river originates and section B to J are the downstream adjacent parts (Table 3 and Figure 5).

The sinuosity value decreases gradually from 1989 to 2017. The river shows high sinuosity in H section of 1989 bank. The lowest sinuosity is seen in D section of 2017 bank. High sinuosity (>1.50) value means the part of the channel is meandering while the range between 1.05-1.25 suggests the channel is winding. Sediment transport, bed load together with the slope of the floodplain are the basic factors that influence sinuosity (Smith, 1998).

Bank shift

Decadal bank shifts of both right and left bank have been assessed section wise (Table 4 and Figure 6). The bank shift is quite fluctuating in each decade. However, compared to 1989-1999, the other two decades show greater shift. There is a high shift of 42.7 m in the right bank of F-section during the decade 1999-2009. The shift may result due to the river flowing into wider plain after flowing from the narrow channel. Similarly, rivers

tend to spread laterally towards the lower region of the valley. Therefore, most of the high values of bank shifts are seen in lower sections.

Table 3, Decadal sinuosity of Seti

S. No	Section	Left_1989	Right_1989	Left_1999	Right_1999	Left_2009	Right_2009	Left_2017	Right_2017
1.	A	1.56	1.58	1.54	1.59	1.51	1.50	1.63	1.64
2.	B	1.38	1.39	1.36	1.34	1.38	1.35	1.38	1.47
3.	C	1.74	1.74	1.74	1.68	1.68	1.73	1.54	1.54
4.	D	1.45	1.44	1.42	1.39	1.36	1.38	1.26	1.24
5.	E	1.73	1.70	1.75	1.71	1.64	1.64	1.57	1.59
6.	F	1.40	1.38	1.38	1.32	1.31	1.28	1.28	1.32
7.	G	1.52	1.46	1.53	1.49	1.48	1.45	1.37	1.35
8.	H	1.79	1.81	1.71	1.79	1.66	1.74	1.64	1.53
9.	I	1.45	1.39	1.47	1.45	1.47	1.42	1.31	1.29
10	J	1.68	1.68	1.79	1.68	1.65	1.67	1.52	1.42

Table 4, Decadal Bank shift of Seti in meters

S. No	Section	1989 to 1999_L	1989 to 1999_R	1999 to 2009_L	1999 to 2009_R	2009 to 2017_L	2009 to 2017_R
1	A	11.5	9.5	13.1	12.5	18.9	19.3
2	B	7.7	6.7	10.4	12.2	20.5	19.2
3	C	7.9	8.1	13.1	10.3	14.9	17.1
4	D	8.2	10.0	9.1	9.1	11.5	13.1
5	E	9.6	9.8	11.1	12.2	17.2	17.8
6	F	15.5	25.1	29.9	42.7	27.9	19.7
7	G	15.5	16.7	17.1	17.3	24.7	20.9
8	H	12.5	12.3	16.6	19.1	22.8	23.7
9	I	24.8	30.1	22.6	19.4	24.5	27.4
10	J	14.5	15.1	36.1	20.2	36.7	23.6

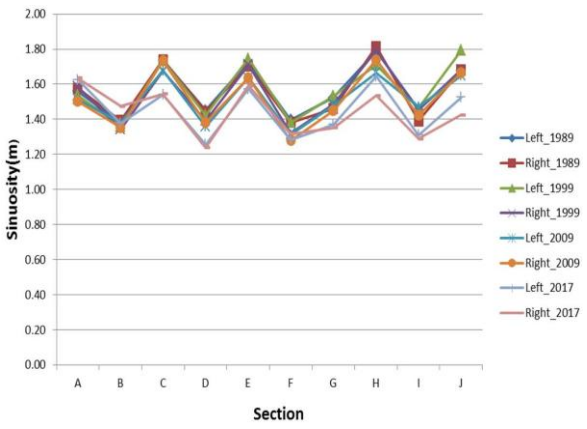

Figure 5, Section wise sinuosity of Seti from 1989 to 2017

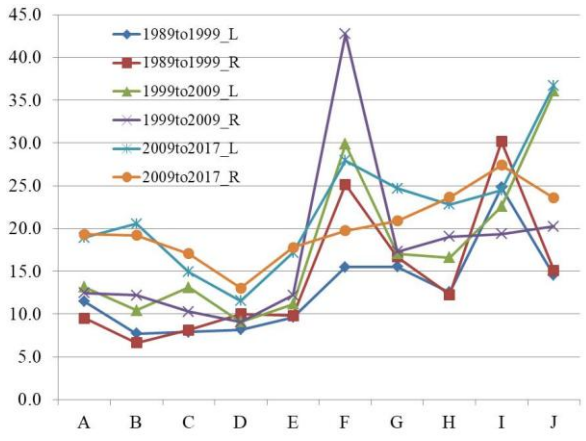

Figure 6, Section wise bank shift of Seti from 1989 to 2017

Threshold values of land class

The following threshold values were determined and land classes were separated accordingly with the help of the three major indices. Table 5 shows the land use classes and their respective threshold values (reflectance).

Table 5, Land use classes and their reflectance

S. No.	Land Class	Indices Used	Threshold values (Reflectance)
1.	Built up area	NDVI	0.11-0.3
2.	Barren land		0.3-0.36
3.	Agriculture and Grassland		0.36-0.5
4.	Shrub and forest		>0.5
5.	Water Bodies	NDWI	>0.35
6.	Snow and glacier	NDSI	>0.5

LULC classification

Land use cover classification was done for the following years and was divided into 6 major classes. Table 6 shows the area occupied by each class in the following years.

Table 6, The area occupied by land use class in sq km

S. No.	Land Class	1989	1999	2009	2017
1	Water Body	7.60	7.9	7.34	8.34
2	Builtup Area	32.44	54.39	74.15	80.98
3	Barren land	353.802	341	355.66	332.07
4	Agriculture and grassland	251.207	274.03	299.76	320.15
5	Shrub and forest	984.753	916.48	911.50	889.05
6	Snow and Glacier	458.052	495.95	439.37	477.55
Total		2088	2088	2088	2088

Figure 7, Figure 8, Figure 9 and Figure 10 respectively show the LULC of Kaski from the 1989 to 2017. The overall result delineates that there was a huge change in shrub and forest area from 984.753km^2 (1989) to 889.05km^2 (2017). The land class that was least changed was water bodies from 7.60 km2 in 1989 to 8.34 km^2 in 2017.The barren land decreased from 353.802 to 332.07 km^2 while agriculture land seems to increase proportionately every decade starting from 251.207 km^2 in 1989 to 320.15 km^2 in 2017. Builtup area seems to increase gradually from 32.44 to 80.98 km^2. The decreasing trend of shrub and forest land seems prominent in every decade. The area coverage of snow and glaciers seems to fluctuate every decade. However, there is an overall increase in its area from 458.052 km^2 (1989) to 477.55 km^2 (2017). These changes can mainly be attributed to anthropogenic activities and to some extent the natural causes as well. Rapid urbanization is one of the main causes that drives changes in land cover patterns (Xiao et al., 2006). To meet the demands of increasing population the vegetation land is rapidly cleared out and is replaced with builtup areas. Such trend is seen in the above results too. With the decadal increase in builtup areas, a decrease in shrub and forest area is quite evident. The barren land has also decreased subsequently and resulting into conversion of built up areas.

LULC map of Kaski indicates a lot of changes in the land use and cover pattern of the area under study in different periods of time. From Figure 7, the initial pattern of land use and cover of the area can be noticed, which is dominated by extensive presence of shrubs, forest, and glacial areas with few infrastructural developments. In Figure 8, an increase in built-up areas has been observed, mainly in the southern and central part of the district. Figures 7, Figure 8, Figure 9 and Figure 10 present the LULC maps of Kaski for 1989, 1999, 2009, and 2017, respectively, whereas Figure 11 summarizes the temporal changes in the area of each land-cover class..

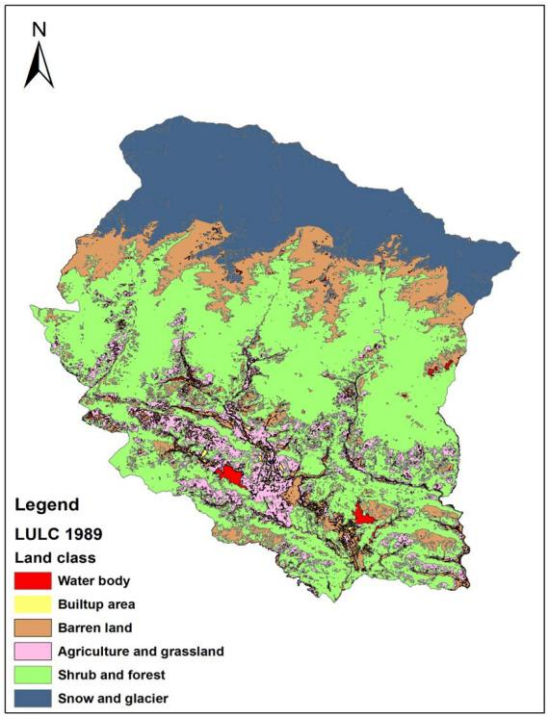

Figure 7, LULC of Kaski in 1989

Natural phenomenon such as floods, change in river courses and other such river and Riverine hazards also trigger land use changes. The 2012 Seti flash flood resulted in conversion of the settlement area into the debris filled land. The meandering pattern of Seti is also responsible for the conversion of cultivated land into sand area. Certain areas of the district, especially Pokhara city is vulnerable to flooding, riverbank erosion and slope undercutting and sinkhole hazards since the river flows beneath the city weakening/undermining the stability of the ground materials.

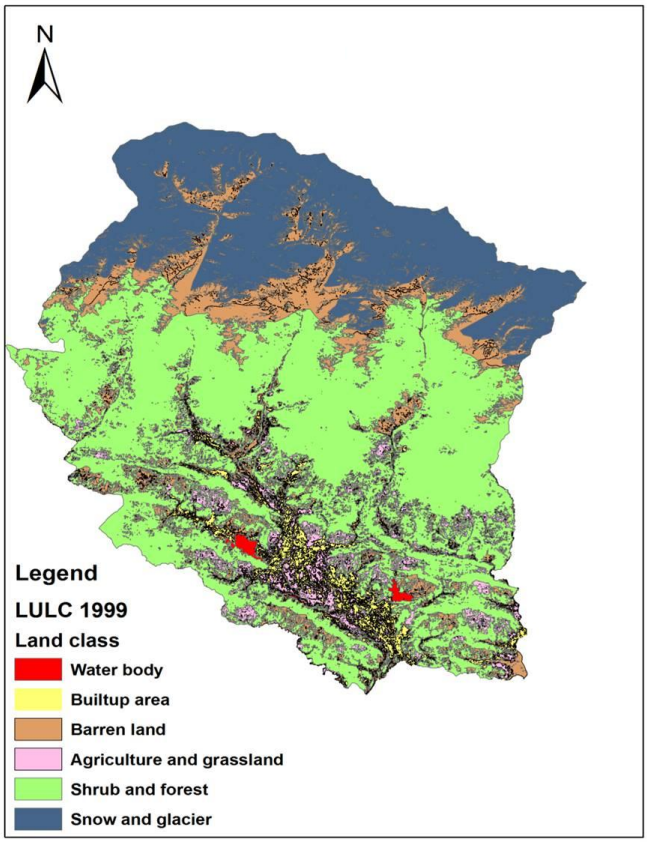

Figure 8, LULC of Kaski in 1999

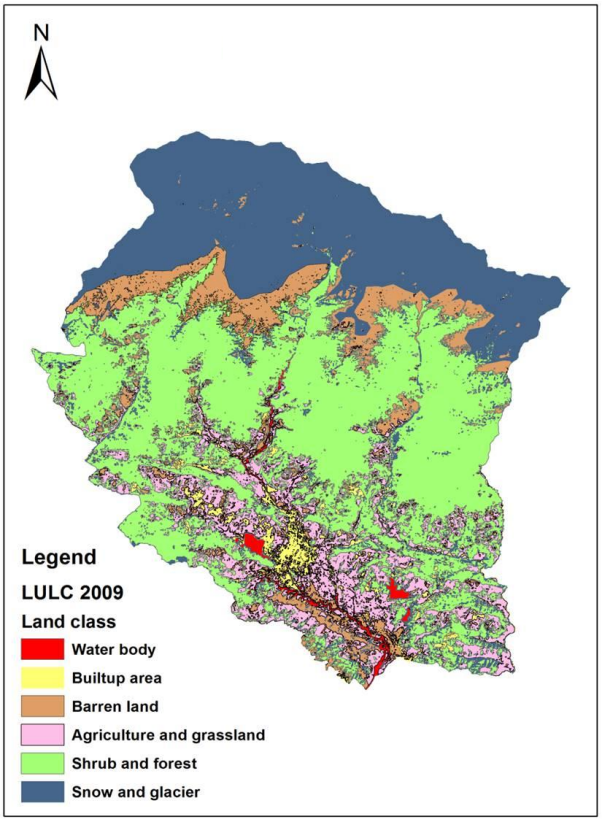

Figure 9, LULC of Kaski in 2009

Agricultural land is most vulnerable to such Riverine hazards, including some settlements located on unstable or flood-prone terrain. Such events are eventually responsible changing landforms and land patterns (Rimal et al., 2015).

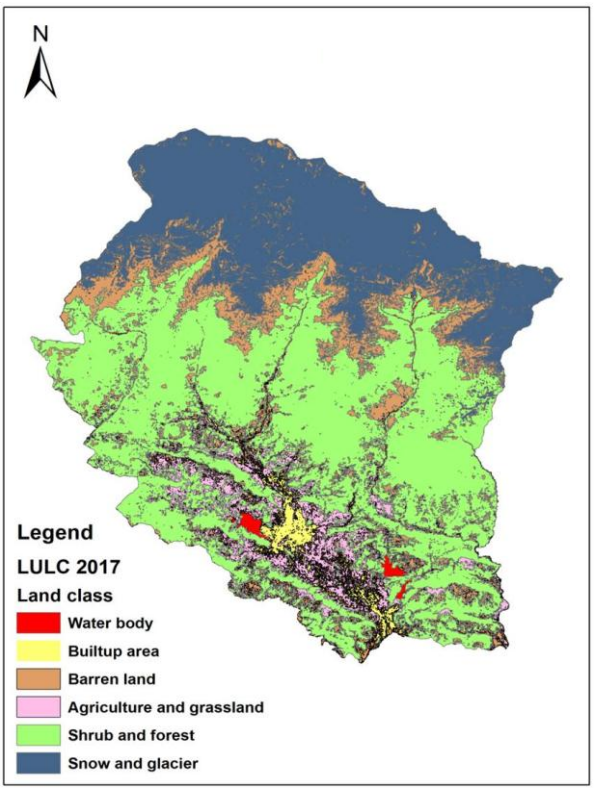

Figure 10, LULC of Kaski in 2017

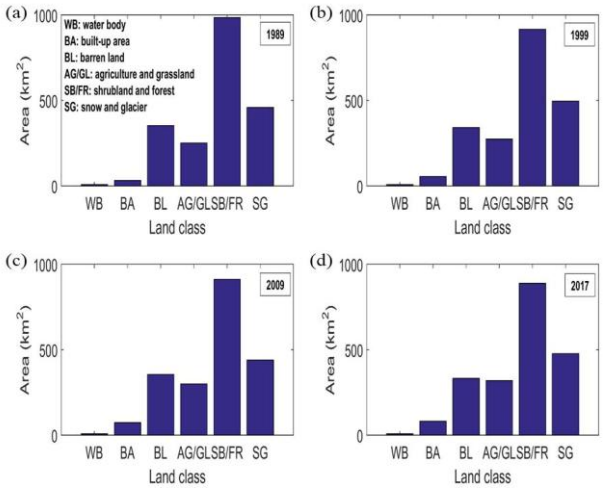

Figure 11, Area covered by each land class between the period of 1989-2017 (a) In 1989, (b) In 1999, (c) In 2009 and (d) In 2017

Furthermore, the interaction between the Seti River and surrounding landforms reveals the fragile geomorphic stability of the region. Continuous erosion, sediment deposition, and channel shifting have altered the landscape and affected local livelihoods, underscoring the need for integrated river basin management and sustainable land use planning in Kaski district. In particular: (a) The overall tendency towards a reduction in sinuosity in sections D, H, and J may be associated with increased straightening of the channel, which may lead to higher flow velocities and flood risk

downstream. (b) The bank shifts, especially the 42.7 m bank shift at Section F (1999–2009) may indicate the presence of some level of channel instability with the potential danger to nearby agricultural and built-up areas in the valley. (c) A very slight increase in water body size may point to channel widening. (d) The nearly doubled built-up area (32.44 km^2 to 80.98 km^2) will further increase people's exposure to flood risk. (e) The reduction in shrubs and forests will reduce the amount of interception and will make more land available for erosion and surface runoff. (f) The small net increase in the amount of snow and glaciers on the territory of the river is locally unusual when compared to global trends; it is explained by the inter-decadal fluctuations in snow cover mapping using Landsat satellite images, not by any proven glacier expansion.

Conclusion

This study employed GIS and remote sensing techniques to evaluate decadal changes in river morphology and land use/land cover (LULC) in the Seti River corridor, Kaski District, Nepal, from 1989 to 2017. The results demonstrate the effectiveness of geospatial technologies for long-term environmental monitoring and provide valuable insights into the interactions between river dynamics and landscape transformation.

The LULC analysis revealed significant changes over the study period. Shrubland and forest cover declined from 47.17% in 1989 to 42.17% in 2017, indicating continued land cover transformation. In contrast, built-up areas expanded markedly from 32.44 km^2 to 80.98 km^2, reflecting rapid urbanization and infrastructure development. Agricultural land also increased gradually, suggesting continued cultivation expansion. Snow and glacier cover showed interdecadal fluctuations with a slight overall increase; however, this trend should be interpreted cautiously because Landsat-based snow classification is influenced by seasonal variation and classification uncertainty.

Morphological analysis indicated that the Seti River largely maintained its meandering planform, although localized channel adjustments were evident. Reduced sinuosity at Sections D, H, and J indicates channel straightening, while spatial variations in bank migration highlight the river's dynamic nature. The maximum bank shift of 42.7 m occurred at Section F during 1999–2009, demonstrating active lateral migration. An increase in water surface area further suggests localized channel widening associated with erosion, sediment redistribution, and flood processes. Overall, the study highlights increasing human influence through declining shrubland and forest cover and expanding built-up and agricultural areas, while confirming that the Seti River remains geomorphologically active. These findings provide valuable baseline information for sustainable land use planning, river corridor management, flood hazard mitigation, and environmental conservation in the rapidly developing Seti River basin and other Himalayan river systems.

Article Note

This article is a full-length paper developed from **Extended Abstract #211**, entitled "**Spatio-Temporal Changes in River Dynamics and Land Cover Along the Seti River Floodplain, Kaski District, Nepal (1989–2017)**", which was presented at the 15th Asian Regional Conference of the International Association for Engineering Geology and the Environment (ARC-15 of IAEG), held in Kathmandu, Nepal, from 27 to 29 November 2025.

Reference

AEPC. (2017). Alternative Energy Promotion Centre. Available at: http://aepc.gov.np/

Barnsley, M. (1999). Digital remotely-sensed data and their characteristics. In Geographical Information Systems (Vol. 1, pp. 451–466). Available at: https://www.geos.ed.ac.uk/~gisteac/gis_book_abridged/files/ch32.pdf

Burrough, P. A. and McDonnell, R. A. (1998). Principles of Geographical Information Systems. Oxford University Press, Oxford, 333p.

Deng, J. S., Wang, K., Hong, Y., and Qi, J. G. (2009). Spatio-temporal dynamics and evolution of land use change and landscape pattern in response to rapid urbanization. Landscape and Urban Planning, 92(3), 187–198. https://doi.org/10.1016/j.landurbplan.2009.05.001

Dufour, S., Rinaldi, M., Piégay, H., and Michalon, A. (2015). How do river dynamics and human influences affect the landscape pattern of fluvial corridors? Lessons from the Magra River, Central-Northern Italy. Landscape and Urban Planning, 134, 107–118. https://doi.org/10.1016/j.landurbplan.2014.10.007

Ebisemiju, F. S. (1994). The sinuosity of alluvial river channels in the seasonally wet tropical environment: Case study of River Elemi, southwestern Nigeria. Catena, 21(1), 13–25. https://doi.org/10.1016/0341-8162(94)90028-0

Govaerts, B., and Verhulst, N. (2010). The normalized difference vegetation index (NDVI) GreenSeeker™ handheld sensor: Toward the integrated evaluation of crop management. Part A—Concepts and case studies. Available at: https://www.nue.okstate.edu/GreenSeeker/NDVI-PartA-mayo.pdf

Hassan, Z., Shabbir, R., Ahmad, S. S., Malik, A. H., Aziz, N., Butt, A., and Erum, S. (2016). Dynamics of land use and land cover change (LULCC) using geospatial techniques: A case study of Islamabad, Pakistan. SpringerPlus, 5(1), 1–11. Available at:

https://link.springer.com/article/10.1186/s40064-016-2414-z

Hazarika, N., Das, A. K., and Borah, S. B. (2015). Assessing land-use changes driven by river dynamics in chronically flood-affected Upper Brahmaputra plains, India, using RS-GIS techniques. The Egyptian Journal of Remote Sensing and Space Science, 18(1), 107–118. https://doi.org/10.1016/j.ejrs.2015.02.001

HIMALDOC. (2017). Retrieved September 3, 2017, from http://lib.icimod.org/Kalliola, R., and Puhakka, M. (1988). River dynamics and vegetation mosaicism: A case study of the River Kamajohka, northernmost Finland. Journal of Biogeography, 703–719. https://doi.org/10.2307/2845334

Klöcking, B., and Haberlandt, U. (2002). Impact of land use changes on water dynamics: A case study in temperate meso- and macroscale river basins. Physics and Chemistry of the Earth, Parts A/B/C, 27(9), 619–629. https://doi.org/10.1016/S1474-7065(02)00046-3

Lambin, E. F., Geist, H. J., and Lepers, E. (2003). Dynamics of land-use and land-cover change in tropical regions. Annual Review of Environment and Resources, 28(1), 205–241. https://doi.org/10.1146/annurev.energy.28.050302.105459

Matheussen, B., Kirschbaum, R. L., Goodman, I. A., O'Donnell, G. M., and Lettenmaier, D. P. (2000). Effects of land cover change on streamflow in the interior Columbia River Basin (USA and Canada). Hydrological Processes, 14(5), 867–885. https://doi.org/10.1002/(SICI)1099-1085(20000415)14:5%3C867::AID-HYP975%3E3.0.CO;2-5

McFeeters, S. K. (1996). The use of the Normalized Difference Water Index (NDWI) in the delineation of open water features. International Journal of Remote Sensing, 17(7), 1425–1432. https://doi.org/10.1080/01431169608948714

Mohan, M., Pathan, S. K., Narendrareddy, K., Kandya, A., and Pandey, S. (2011). Dynamics of urbanization and its impact on land-use/land-cover: A case study of megacity Delhi. Journal of Environmental Protection, 2(9), 1274–1283. https://doi.org/10.4236/jep.2011.29147

Müller, N. (1996). River dynamics and floodplain vegetation and their alterations due to human impact. River Systems, 9(3-4), 477-512. https://doi.org/10.1127/lr/9/1996/477

Petchprayoon, P., Blanken, P. D., Ekkawatpanit, C. and Hussein, K. (2010). Hydrological impacts of land use/land cover change in a large river basin in central–northern Thailand. International Journal of Climatology, 30(13), 1917-1930. https://doi.org/10.1002/joc.2131

Riggs, G. A., Hall, D. K., and Salomonson, V. V. (1994). A snow index for the Landsat thematic mapper and Moderate Resolution Imaging Spectroradiometer. In Geoscience and Remote Sensing Symposium, 1994. IGARSS '94. Surface and Atmospheric Remote Sensing: Technologies, Data Analysis and Interpretation (Vol. 4, pp. 1942–1944). https://doi.org/10.1109/IGARSS.1994.399618

Rimal, B., Baral, H., Stork, N. E., Paudyal, K. and Rijal, S. (2015). Growing city and rapid land use transition: Assessing multiple hazards and risks in the Pokhara Valley, Nepal. Land, 4(4), 957-978. https://doi.org/10.3390/land4040957

Rouse, H. (1937). Modern conceptions of the mechanics of fluid turbulence. Transactions of the American Society of Civil Engineers, 102, 463-543. https://doi.org/10.1061/TACEAT.0004872

Shrestha, P. (2010). Climate change impact on river dynamics of the Bagmati Basin, Kathmandu, Nepal. Report submitted to the National Adaptation Programme of Action (NAPA) to Climate Change Project, Government of Nepal.

Smith, C. E. (1998). Modeling high sinuosity meanders in a small flume. Geomorphology, 25(1), 19–30. https://doi.org/10.1016/S0169-555X(98)00029-4

Walker, R., and Homma, A. K. O. (1996). Land use and land cover dynamics in the Brazilian Amazon: An overview. Ecological Economics, 18(1), 67–80. https://doi.org/10.1016/0921-8009(96)00033-X

Wang, J., Rich, P. M., Price, K. P., and Kettle, W. D. (2005). Relations between NDVI, grassland production, and crop yield in the central Great Plains. Geocarto International, 20(3), 5–11. https://doi.org/10.1080/10106040508542350

Wu, W. (2010). Computational river dynamics. CRC Press. 509p.

Xiao, J., Shen, Y., Ge, J., Tateishi, R., Tang, C., Liang, Y., and Huang, Z. (2006). Evaluating urban expansion and land use change in Shijiazhuang, China, by using GIS and remote sensing. Landscape and Urban Planning, 75(1), 69–80. https://doi.org/10.1016/j.landurbplan.2004.12.005

Yang, A. Y., Wright, J., Ma, Y., and Sastry, S. S. (2008). Unsupervised segmentation of natural images via lossy data compression. Computer Vision and Image Understanding, 110(2), 212–225. Available at: https://people.eecs.berkeley.edu/~sastry/pubs/Pdfs%20of%202008/YangUnsupervised2008.pdf

Zewdu, S., Suryabhagavan, K. V., and Balakrishnan, M. (2016). Land-use/land-cover dynamics in Sego Irrigation Farm, southern Ethiopia: A comparison of temporal soil salinization using geospatial tools. Journal of the Saudi Society of Agricultural Sciences, 15(1), 91–97. https://doi.org/10.1016/j.jssas.2014.03.001